Multiatom resonant photoemission

A. W. Kay,[1,2] F. J. Garcia de Abajo,[2,3] S.-H. Yang,[2] E. Arenholz,[4] B. S. Mun,[1,2] N. Mannella,[1,2] Z. Hussain,[4] M. A. Van Hove,[1,2] and C. S. Fadley[1,2]

[1]*Department of Physics, University of California-Davis, Davis, California 95616*
[2]*Materials Sciences Division, Lawrence Berkeley National Laboratory, Berkeley, California 94720*
[3]*Centro Mixto CSIC-UPV/EHU, San Sebastian, Spain*
[4]*Advanced Light Source, Lawrence Berkeley National Laboratory, Berkeley, California 94720*

We present experimental and theoretical results related to multiatom resonant photoemission, in which the photoelectron intensity from a core level on one atom is influenced by a core-level absorption resonance on another. We point out that some prior experimental data has been strongly influenced by detector nonlinearity and that the effects seen in new corrected data are smaller and of different form. Corrected data are found to be well described by an extension of resonant photoemission theory to the interatomic case, provided that interactions beyond the usual second-order Kramers-Heisenberg treatment are included. This microscopic theory is also found to simplify under certain conditions so as to yield results equivalent to a classical x-ray optical approach, with the latter providing an alternative, although less detailed and general, physical picture of these effects. The potential utility of these effects as near-neighbor probes, as well as their implications for x-ray emission and x-ray scattering experiments, are also discussed.

PACS number(s): 79.60.−i, 68.35.−p, 78.20.Ci, 78.70.Dm

I. INTRODUCTION

In several recent papers by our group,[1–5] it has been suggested that photoemission associated with a certain core electronic level of a given atom ''*A*'' can be significantly enhanced in intensity by tuning the photon energy through core-level absorption edges of a near-neighbor atom ''*B*.'' The apparent enhancements seen in experimental data for several metal oxides (e.g., MnO, Fe_2O_3, and $La_{0.7}Sr_{0.3}MnO_3$),[1,2] as well as in a series of Cr/Fe alloys and bilayers[3b] were very large, ranging up to 40–100% of the nonresonant intensity, and they were furthermore observed to follow closely the x-ray absorption coefficient of atom *B* in shape.[1–3] The effects observed have been termed multiatom resonant photoemission (MARPE) to distinguish them from the better-known intra-atomic single-atom resonant photoemission (SARPE). Similar effects have also been reported in other transition metal compounds[6] and in adsorbates[7] by other groups. Analogous and presumed related enhancements also appeared to be present in the secondary decay processes of Auger electron and fluorescent x-ray emission, again tracking very closely the x-ray absorption coefficient in form.[4] A theoretical model based on an extension of normal SARPE theory has also been presented to describe these results, and the first comparisons of calculations based on it yielded encouraging agreement with experiment.[5] The potential utility of such effects for studying near-neighbor atom identities and bonding have also been pointed out.[1–4] Independent of this work on *core-core* multiatom resonant photoemission, other groups have reported the enhancement of *valence* photoemission intensities primarily associated with emission from a certain atom *A* upon tuning the photon energy through the core-level absorption edges of a nearby atom *B*, with this work including measurements near solid-solid interfaces[8,9] and on a free molecule.[10] No attempts have as yet been made to theoretically model this latter type of valence-core MARPE effect.

In this paper, we first point out that the measurement of the core-core multiatom resonant photoemission effects mentioned above (or indeed any resonant-or nonresonant-photoemission effect) must be carried out with extreme care to avoid nonlinearities in the electron detector response, and illustrate these effects by carrying out corrections on a few representative data sets for O 1 s emission from MnO in resonance with the Mn 2*p* excitations. The corrected results are found to show significantly smaller MARPE effects on photoelectron intensities, with shapes now considerably different from the x-ray absorption coefficient. In addition, theoretical calculations based on the previously discussed microscopic model,[5] and on a simpler classical theory of x-ray optics[11] are presented and found to yield excellent agreement with the remaining experimental effects, thus clarifying the physics involved. We also comment on the implications of this work for other recent core-core and valence-core MARPE measurements,[6–10,12,13] as well as for x-ray emission[4,14] and x-ray scattering experiments.

II. EXPERIMENTAL PROCEDURE AND DATA ANALYSIS

All photoelectrons were analyzed in energy and detected with a Scienta ES200 electron spectrometer system,[15a] as situated either on a bend-magnet beamline[15b] (9.3.2) or an undulator beamline (4.0.2) at the Berkeley Advanced Light Source. The final multichannel detection system used is that provided as part of the standard equipment by the manufacturer: a microchannel plate multiplier followed by a phosphor screen at high voltage in a vacuum, and a charge-coupled device (CCD) video camera outside of the vacuum to finally convert light pulses into counts. We have operated this detector in the ''greyscale'' or ''analog'' mode in which an integrated CCD charge is used for counting, rather than in the alternate ''black-and-white'' or ''digital mode,'' in

63 115119-1

which individual pulses are counted. The detector has in addition been used as delivered and installed by the manufacturer; thus, the discriminator setting was left at its recommended value at setup. This spectrometer and detector system is furthermore the same as that used by some other groups attempting to measure multiatom resonant photoemission effects.[6,7] We have in the present study calibrated our detector system in both analog and black-and-white modes by using a standard x-ray tube with a continuously variable emission current at a fixed high voltage, verifying initially that the total electron current from the sample tracked linearly with the emission current: thus, the emission current is directly proportional to the x-ray flux incident on the sample. The general methodology for this calibration and the final correction of spectra is discussed elsewhere,[16,17] and in one case, discussed together with previous data for a similar electron detection system.[16]

III. RESULTS AND DISCUSSION

In Fig. 1(a) and its inset, we show the measured (dashed curve) vs ideal or ''true'' (straight line) response of this detector as used in analog mode over a countrate range spanning 0 to 500 Hz in a typical x-y pixel of the approximately 70 000 pixels in the CCD camera used in normal operation. We have verified that all spatial regions of the detector behave in essentially the same manner,[17] so the performance shown can be applied over the entire active region. The inset makes it clear that there is curvature in the response, with falloff and incipient saturation being seen as the countrate increases. Although one might then expect linearity for the lowest countrates, the blowup of the 0–20 Hz region (the maximum used in all of our measurements to avoid falloff and saturation) shown in the main figure makes it clear that there is still significant nonlinearity, including what is found to be a quadratic component as compared to an ideal detector with linear response that we define to be equal to that of the real detector in the limit of zero countrate (solid line of the unit slope in the figure and inset). For reference, the 20 Hz per pixel rate would correspond to a global countrate of 1.4 MHz (before a ''multiple counting'' divisor introduced by the manufacturer's software is applied) for the entire useable portion of the detector phosphor and if the phosphor were evenly illuminated.

Thus, although measured and true rates can be conveniently defined to yield the same unit slope as countrates go to zero, the measured rates deviate significantly from linearity, showing quadratic overcounting over the full range of our earlier measurements. Almost identical quadratic effects were also found in the black-and-white mode, although this mode was not used in our measurements.[17] An additional effect of such quadratic overcounting is the narrowing or broadening of the photoelectron peaks in energy as a high-intensity resonance is passed, depending on which portion of the nonlinear response a given photon energy scan occupies, and we have in prior work[1–4] also used the additional criterion of constant peak width over an energy scan to try to minimize nonlinearities. However, this criterion of constant peak width proves to be inadequate for avoiding spurious

effects on peak intensity measurements. Using methods described in detail elsewhere,[16,17] the detector response curve in Fig. 1(a) can be turned into an efficiency, and the inverse of this efficiency then used to correct individual spectra in a point-by-point fashion. Although it is possible that adjusting the discriminator setting on the detector could reduce these nonlinearities, several other groups appear to have encountered the same type of nonlinearity with the standard manufacturer's settings.[6,7,18] It has also been suggested that a change in the CCD camera might improve this behavior,[19] and this is another direction for future investigation.

Both uncorrected (as measured) and corrected (''true'') spectra are shown in Fig. 1(b) for O $1s$ emission from MnO, where the photon energies of 637.6 and 640.2 eV have been chosen to be just below the strong Mn $2p_{3/2}$ resonance and just on this resonance, respectively.[1] Because of the significantly increased background level associated with secondary decay processes and inelastically scattered electrons arising from the Mn $2p_{3/2}$ absorption, which in turn forces the detector countrate further up its nonlinear response curve, the correction procedure acts to a greater degree on resonance. Thus, the intensity on resonance is artificially enhanced. In fact, in order to decrease these nonlinear correction effects to negligibly low levels, we have found in data not shown here that the countrates had to be lowered by another order of magnitude from our prior typical operating points, or to about 2 Hz per pixel.[17]

In Fig. 1(c), we now show uncorrected and corrected O $1s$ intensities, measured as areas by fitting analytical peak shapes plus backgrounds to spectra such as those in Fig. 1(b), as a function of photon energy, with curves such as these being discussed previously in terms of multiatom resonant photoemission.[1–4] It is clear that the uncorrected MARPE scan follows very closely the previously published x-ray absorption curve for MnO in the Mn $2p_{3/2}$ region,[1–3] which we also show in Fig. 1(c) as derived from the inelastic electron background under the O $1s$ spectra,[1] with about a 32% enhancement of intensity of the O $1s$ intensity at the Mn $2p_{3/2}$ peak.[1–4] However, the corrected MARPE scan shows a much smaller effect of about 12% in overall excursion, and also of a much different form, being negative just below the resonance and then going positive. In data obtained at other x-ray incidence angles over the range of 5–30°,[17] we have also found that these corrected effects are strongly dependent on angle, being largest for more grazing x-ray incidence angles, such as the analogous results for 10° shown in Fig. 1(c), which exhibit about 37% overall excursion, and quickly decaying in magnitude as this angle is increased. We estimate our overall systematic error in the corrected spectra as ±2%, with some channel-to-channel statistical scatter around this.

As a final point on this correction, it appears that, with constant UHV conditions of operation, the correction function does not change significantly over a period of months, with older data obtained via the same detector setup showing reasonable correctability. However, the correction function should in any case be checked frequently to avoid any drifts with time.

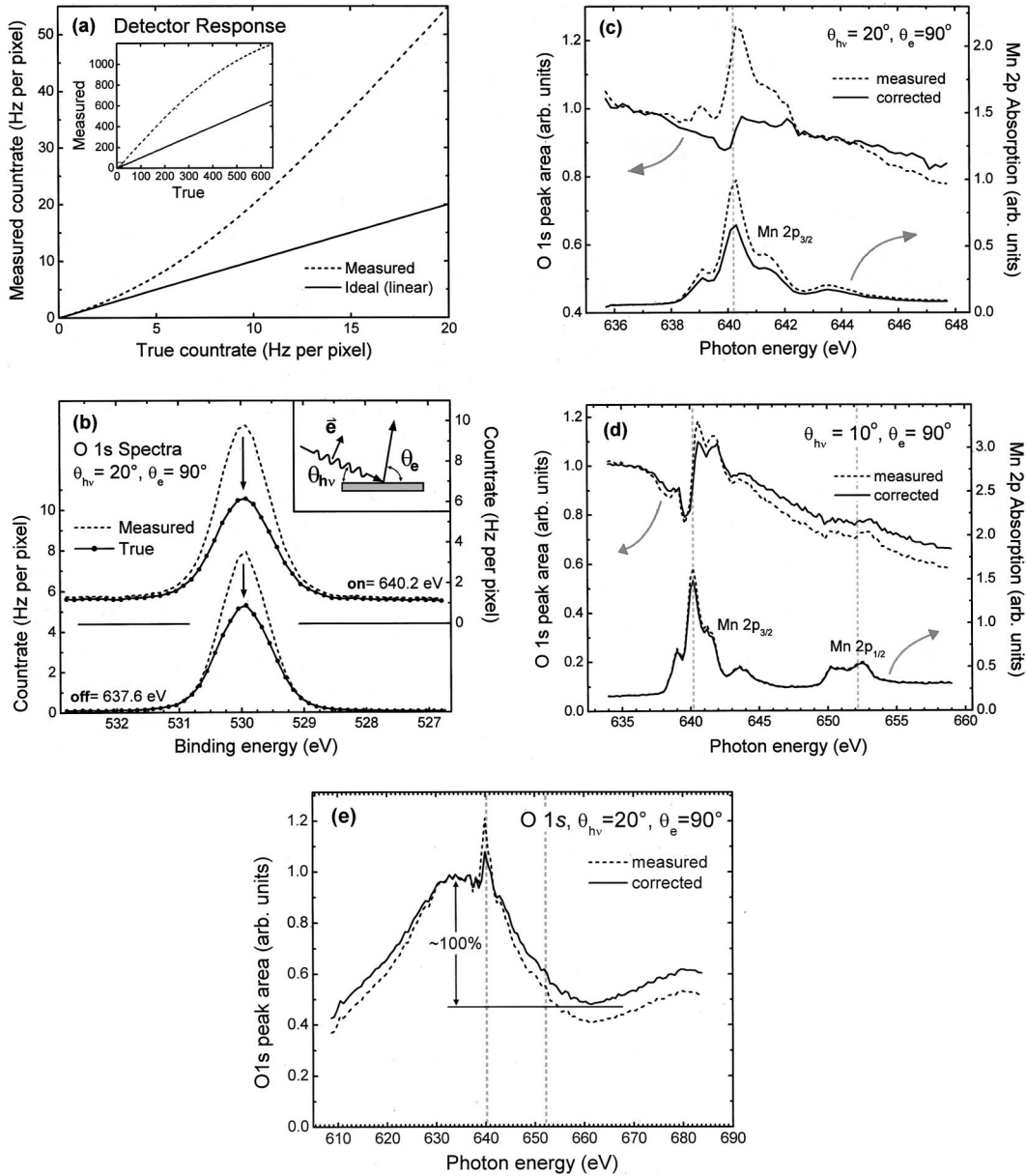It is thus clear that detector nonlinearity can have a dra-

FIG. 1. (a) The measured response function of our multichannel detection system (dashed curves), as plotted against the linear reference of an ideal detector (solid lines). The ordinate is measured counts per energy pixel, and the abscissa is proportional to the "true countrate" expected, which is in turn proportional to the emission current of the x-ray tube and, thus, incident x-ray flux. The inset shows the same kind of plot over a much broader countrate range. The solid lines for the ideal detector are chosen to asymptotically agree with the slope of the measured curve at the lowest countrates, although the final corrected results in (b)–(d) do not depend on this choice of reference. (b) O $1s$ spectra from MnO(001) off resonance (photon energy $h\nu = 637.6$ eV) and on resonance ($h\nu = 640.2$ eV) are shown before (dashed curves) and after (solid curves) applying the correction for detector nonlinearity. The inset shows the experimental geometry, with x-ray incidence for this case at $\theta_{h\nu} = 20°$ and electron exit along the surface normal at $\theta_e = 90°$. The radiation is linear p-polarized, with the electric field vector **e** lying in the plane of the figure. (c) O $1s$ intensities derived from fitting analytical peak shapes to uncorrected (dashed curve) and corrected (solid curve) spectra such as those in (b) as a function of photon energy over the Mn $2p_{3/2}$ absorption range and still for $\theta_{h\nu} = 20°$, $\theta_e = 90°$. Also shown in the bottom of the panel is the Mn $2p_{3/2}$ absorption coefficient, as measured via the inelastic background underneath the O $1s$ peak. (d) As (c), but for $\theta_{h\nu} = 10°$, $\theta_e = 90°$ and extending over the full Mn $2p_{3/2,1/2}$ range. The countrates here were actually higher than in (c), but spanned a smaller portion of the detector dynamic range, and hence, the corrections are smaller in magnitude. (e) As (b), but with a broader energy range that clearly shows the oscillation associated with scanned-energy photoelectron diffraction.

matic effect on such measurements, with the solid curves in Figs. 1(b), 1(c), and 1(d) now representing much more accurately any effects beyond a simple one-electron picture of O $1s$ emission from MnO. Without such interatomic effects,

one should observe a simple smooth curve of negative slope over this region in energy due to a combination of subshell cross section and electron inelastic attenuation length variation,[11,20] as perhaps modulated by energy-dependent

photoelectron diffraction (PD).[17,21] The effects of scanned-energy photoelectron diffraction are in fact clearly shown in Fig. 1(e), which represents a broader energy scan for the same experimental conditions as in Fig. 1(c). Here, the long-wavelength oscillation with a maximum at ∼634 eV has been verified via theoretical calculations to be due to PD effects.[17]

We also note that, in addition to affecting photoemission results, prior measurements of secondary Auger and x-ray emission effects[4] also appear to have been strongly influenced by such detector nonlinearities, for the former, just as for the photoelectron case due to the identical instrumentation, and for the latter via an x-ray absorption coefficient necessary for a self-absorption correction that was measured via secondary electrons in the same electron spectrometer.

Beyond the particular case of MARPE considered here, we also point out that such detector nonlinearities need to be corrected for and/or minimized in any use of this detector system for quantitative peak intensity analysis, as any comparison of intensities obtained over a range of countrates, even in a single spectrum, can be significantly altered by these effects.

IV. THEORY AND DISCUSSION

A. Interatomic resonant photoemission model

We now consider several levels of theory in order to explain the remaining effects that link the O 1s intensity to the Mn 2p absorption process as seen in Figs. 1(c) and 1(d), first considering these effects via a prior microscopic many-body theoretical treatment of MARPE based on a resonant photoemission model,[5] and then showing that this approach can be successively simplified for the case at hand to yield results essentially identical to those from classical x-ray optical theory. Focusing still on the case of O 1s photoemission from MnO(001) and the system initially prepared in its many-body ground state $|g\rangle$, the contribution of the direct or unscattered wave function to the photoelectron intensity can be written

$$I(\mathbf{k}) \propto |\phi_k^0(\mathbf{r})|^2 \propto \left| \sum_{l\mu} Y_{l\mu}(\hat{\mathbf{k}}) i' h_l^{(+)}(kr) M_{El\mu} \right|^2, \quad (1)$$

where $\mathbf{k}$ is the photoelectron wave vector, $\phi_k^0(\mathbf{r})$ is the wave function at the detector, $Y_{l\mu}$ is a spherical harmonic, $h_l^{(+)}(kr)$ is a spherical Hankel function, and

$$M_{El\mu} = \langle El\mu, O1s | T | g \rangle \quad (2)$$

is the matrix element describing the transition to the final state with a photoelectron $|El\mu\rangle$ of energy $E = \hbar^2 k^2 / 2m$ and an O 1s hole. Final-state photoelectron diffraction effects can also be incorporated in this model by using $M_{El\mu}$ as input for self-consistent multiple-electron-scattering equations.[22]

The transition matrix T can be conveniently expanded in a power series with respect to the perturbation of the radiation field V. One then has[23]

$$T = V + VG_0V + VG_0VG_0V + \cdots, \quad (3)$$

where G_0 is the Green function of the unperturbed solid. If we keep only terms up to second order in V, the part of Eq. (3) that makes a nonzero contribution to Eq. (2) reduces to the well-known Kramers-Heisenberg formula for resonant photoemission[24]

$$T = V_{\text{rad}}^0 + \sum_{j,m} V_{\text{AI}}^j \frac{|m,j\rangle\langle m,j|}{\hbar\omega + E_g - E_m + i\Gamma_m/2} V_{\text{rad}}^j, \quad (4)$$

where V_{rad}^0 is the interaction of the radiation with the emitter, V_{rad}^j is the interaction with the resonating atom j, V_{AI}^i is the autoionizing Coulomb interaction between the emitter and atom j, E_g is the ground state energy, and the sums are over both Mn atoms j and their intermediate many-body states $|m,j\rangle$ of energy E_m and width Γ_m. We have here neglected exchange-type interactions via two-electron autoionization processes like $\langle El\mu; g | V_{\text{AI}}^j | m,j; O1s \rangle$ that would lead to a greater overall similarity with the coulomb-plus-exchange matrix elements describing an interatomic Auger process, but such processes should be negligible for non-nearest neighbors and small for nearest neighbors due to their strict dependence on nonzero orbital overlap. Such orbital overlap is not required for the Coulombic term we have included here,[1,5] which is associated with two-electron processes like $\langle El\mu; g | V_{\text{AI}}^j | O1s; m,j \rangle$. A fully general theory of MARPE should include these exchange effects however. We also point out that the connection between MARPE and an interatomic Auger electron emission is primarily formal, since the same sorts of matrix elements are embedded in the expressions describing both. However, the overall processes are fundamentally different.

We now note two special points that have been considered previously:[5] Retardation effects must be considered in the interaction with the external radiation and in the autoionization interaction [see Eq. (4) in Ref. 5], and the interatomic autoionization interaction must be generalized to the fully relativistic Møller formula used previously in the high-energy Auger theory[25,26] [see Eq. (5) in Ref. 5]. At this level, the treatment should be capable of describing all many-electron interactions up to second order in the perturbation via Eq. (4), or up to arbitrary order via Eq. (3), including those for nearest neighbors with the greatest overlap and thus enhanced many-electron interactions with the emitting atom.

If we now sacrifice some accuracy in describing nearest-neighbor behavior, the autoionization interaction can be conveniently expanded in multipoles that should be valid for resonator distances from the emitter $R_j \gg r_1, r_2$, where r_1 and r_2 are electron-nuclear distances and are of the order of the relevant dimensions of the two core orbitals involved (here O 1s and Mn 2p). With these assumptions, and the further neglect of multipoles higher than dipoles, the effective interaction can be reduced to the following, in which several quantities are written out more explicitly than in prior work[5]

$$V_{\mathrm{AI}}^j \approx e^2 r_1 r_2 \sum_{\mu_1 \mu_2} F_{\mu_1 \mu_2}^{R_j} Y_{1\mu_1}(\hat{\mathbf{r}}_1) Y_{1\mu_2}^*(\hat{\mathbf{r}}_2), \qquad (5)$$

where

$$F_{\mu_1 \mu_2}^R = \frac{-4\pi k^3}{3} \left[\frac{\delta_{\mu_1 \mu_2}}{2\pi} h_0^{(+)}(kR) + h_2^{(+)}(kR) Y_{2\mu_2 - \mu_1}(\hat{\mathbf{R}}) \right.$$

$$\left. \times \langle Y_{1\mu_2} | Y_{2\mu_2 - \mu_1} Y_{1\mu_1} \rangle \right] \qquad (6)$$

and the bracket represents a Gaunt integral with standard normalization.[27] Equations (5) and (6) can also be derived in a more rigorous way using nonrelativistic quantum electrodynamics,[22,28,29] where Eq. (6) is found to be simply proportional to the Green function of the photon field in the transverse gauge,[28] and the remaining short-range longitudinal Coulomb coupling is neglected.[29]

Combining results, we now find, in slightly different notation form, but equivalent meaning to that in Ref. 5

$$M_{E1\mu} = A \langle E1 | r | O1s \rangle \delta_{1,1} \sum_\lambda \varepsilon_\lambda^{\mathrm{eff}} \langle Y_{1\mu} | Y_{1\lambda} | Y_{00} \rangle$$

$$= A \langle E1 | r | O1s \rangle \delta_{1,1} \varepsilon_\mu^{\mathrm{eff}} / \sqrt{4\pi}, \qquad (7)$$

where A is a light-intensity normalization constant,

$$\varepsilon_\lambda^{\mathrm{eff}} = \varepsilon_\lambda - \sum_{\lambda' \mu_2} F_{\lambda \mu_2} \alpha_{\mu_2 \lambda'} \varepsilon_{\lambda'} \qquad (8)$$

is now the effective polarization vector that includes the effect of x-ray scattering at the Mn sites, and the magnitude of the resonance is controlled by a product of a structure-factor type of sum over Mn sites

$$F_{\lambda \mu_2} = \sum_j F_{\lambda \mu_2}^{R_j} e^{i\mathbf{k}_{h\nu} \cdot \mathbf{R}_j}, \qquad (9)$$

and the Mn^{2+} polarizability tensor,

$$\alpha_{\mu_2 \lambda'} = -\frac{4\pi e^2}{3} \sum_m \frac{\langle g | r Y_{1\mu_2}^* | m \rangle \langle m | r Y_{1\lambda'} | g \rangle}{\hbar \omega + E_g - E_m + i\Gamma_m/2}. \qquad (10)$$

The form for the polarizability given here makes it clear that it is directly related to the usual description of resonant photoemission in Eq. (4) and Ref. 24.

The polarizability has been calculated using a configuration interaction scheme for a central Mn^{2+} ion surrounded by six O^{2-} ions in an octahedral cluster,[5,24] with interaction parameters derived previously from fits to both SARPE and x-ray absorption data, and an average over orientations of Mn magnetic moments, since the experiments have been performed above the MnO Néel temperature. In addition, $\alpha_{\mu_2 \lambda'}$ can be well approximated by a quantity averaged over diagonal elements, as $\bar{\alpha} \delta_{\mu_2 \lambda'}$, where $\bar{\alpha} = (\alpha_{-1-1} + \alpha_{00} + \alpha_{11})/3$.[5] The above equations were used in Ref. 5 to calculate O $1s$ intensities. However, all resonant contributions to the O $1s$ intensities [i.e., the second term in Eq. (4)] were incorrectly multiplied by an extra factor of -4 in the computer

calculations. Here, we present corrected theoretical results from this model, as well as results going beyond the earlier approximations used by considering higher-order interactions in Eq. (3), and also compare these two sets of results to a theoretical approach based on more standard x-ray optical theory.

In Fig. 2(a) we compare experimental and theoretical results for the O $1s$ intensity as a function of photon energy and for light incident at an angle of 10° with respect to the surface. The connected points represent the corrected experimental results from Fig. 1(d) and the thin solid curve the theoretical results based on Eq. (3) above. The experimental data show a steeper negative slope than the theory as energy is increased, that we have verified by measurements and calculations, to be due to a combination of decreasing photoelectric cross sections and strong modulations due to photoelectron diffraction [cf. Fig. 1(e)],[17] both well-understood effects.[20,21] If this difference in slope is allowed for, the agreement between experiment and theory is qualitatively good, although the amplitude of the intensity modulations is too small by a factor of 2–3 in theory. Now, going beyond this level of microscopic theory, we note that the remaining terms in the series expansion (3) describe processes in which an incoming photon is scattered by more than one Mn atom before it reaches the O emitter. In particular, they incorporate higher-order Mn-Mn interactions via the Møller formula.[5,25,26] This gives rise to extra terms in the effective polarizability of Eq. (7), which now becomes

$$\varepsilon_\lambda^{\mathrm{eff}} = \varepsilon_\lambda - \bar{\alpha} \sum_{\lambda', j} \mathbf{F}_{\lambda \lambda'}^{R_j} e^{i\mathbf{k}_{h\nu} \cdot \mathbf{R}_j} \varepsilon_{\lambda'}$$

$$+ \bar{\alpha}^2 \sum_{\lambda' \lambda'', jj'} \mathbf{F}_{\lambda \lambda''}^{R_j} \mathbf{F}_{\lambda' \lambda''}^{R_j - R_{j'}} e^{i\mathbf{k}_{h\nu} \cdot \mathbf{R}_{j'}} \varepsilon_{\lambda''} + \cdots, \quad (11)$$

where the first two terms are the same as in Eq. (8) after approximating the polarizability by the average scalar $\bar{\alpha}$. This series can be summed up to an infinite order for a slab formed by a finite set of atomic planes,[22] and a semi-infinite medium can be simulated by using a sufficiently large number of layers. The result obtained in that case for the O $1s$ intensity is shown in Fig. 2(a) as a solid curve. The new terms in Eq. (11) bring the theoretical result much closer to the experimental one, making it evident that it is essential to include what is in effect multiple scattering of the incoming radiation in order to accurately describe such strong soft x-ray resonances. To our knowledge, this point has not been made before in discussing such resonances.

B. Relationship to an x-ray optical (dielectric) model

We now consider the relationship of this microscopic many-body theory to another related theoretical method for dealing with such effects: an x-ray optical approach based on Maxwell's and Fresnel's equations, as described in detail elsewhere.[11,30] Equation (11) involves sums over Mn positions in the MnO crystal. However, the details of the atomic structure of the Mn sublattice should be irrelevant in the limit of long radiation wavelengths λ_x for which phase shifts along the scattered paths can be neglected. In this limit, Eq.
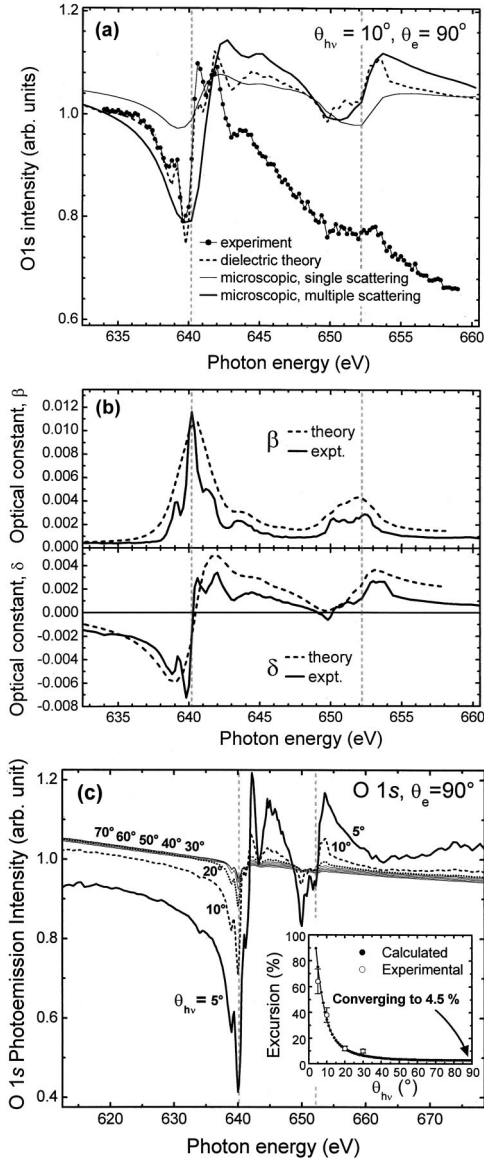
FIG. 2. (a) O 1s intensity from MnO(001) as a function of photon energy and for $\theta_{h\nu}=10°$, $\theta_e=90°$: experimental data (connected points) are compared to theoretical curves calculated using Eq. (8) (thin solid line, second-order microscopic many-body theory=single radiation scattering), Eq. (11) (thick solid line, infinite-order microscopic theory=multiple radiation scattering), and x-ray optical dielectric theory based on Eq. (15) and the experimental constants shown in (b) (dashed curve). (b) The x-ray optical constants δ and β of MnO over the Mn 2p absorption region, as derived from microscopic many-body theory (dashed curves) and from experiment with corrected data for the absorption coefficient μ and Kramers-Kronig analysis. (c) Calculations of the O 1s intensity as a function of photon energy based on the experimental optical constants in (b) and Eq. (15) from x-ray optical theory. Curves are shown for various x-ray incidence angles. The inset shows the normalized magnitude of the negative-to-positive excursion in percent as a function of x-ray incidence angle, as calculated using x-ray optical theory (solid points) and as measured in this study (large open circles).

(11) can be shown to reduce to the polarization vector derived from a macroscopic dielectric description based upon Maxwell's equations, in which the solid is represented by a local frequency-dependent dielectric function ε that is related to the atomic polarizability as $\varepsilon=1+4\pi n_{Mn}\bar{\alpha}$, where n_{Mn} is the density of Mn atoms. This relationship between ε and $\bar{\alpha}$ can be derived from the Clausius-Mossotti relationship with the assumption that $\varepsilon\approx1$, as is reasonable in the soft x-ray region. More specifically, for the case of the Mn2p resonance in MnO, the ratio of the wavelength to the Mn-Mn nearest-neighbor distance is ≈6.1. Therefore, one would expect reasonable results to come out of the macroscopic description. We have here also implicitly assumed that the O atoms contribute only a small amount to the total polarizability in the vicinity of the Mn 2p resonances.[5,22,30b,31]

Thus, an alternative, although more empirically oriented, approach for calculating such effects is to derive the energy-dependent x-ray optical constants $\delta(h\nu)$ and $\beta(h\nu)$ in the index of refraction $n_r=\sqrt{\varepsilon}=1-\delta+i\beta$ (Ref. 32) by measuring the absorption coefficient $\mu(h\nu)=4\pi\beta(h\nu)/\lambda_x$ over the edges in question (here, Mn2p), matching it in the nonresonant region to accurate theoretical and/or experimental data,[30b,31] and then using a Kramers-Kronig analysis to derive δ. These two parameters, as derived experimentally in this study, are shown as a function of photon energy in Fig. 2(b) (solid curves), where they are compared also to the same parameters as derived from the parameterized many-body model (dashed curves). The measured β has been fully corrected for the inelastic attenuation of the outgoing secondary electrons used to measure it via a set of measurements at varying takeoff angles;[17,33] taken together with the corrections for detector nonlinearity, we thus believe that this curve, and the associated δ values, are within $\sim1-2\%$ of the true values. However, such absorption coefficient measurements need to be made with care, so that neither the measurement method (e.g., partial yield, total yield, fluorescence, collection angle) nor nonlinearity in the detector distorts the final curves. The agreement between experiment and theory here is very good, with more fine structure in experiment, as expected. Note also that the variation in the experimental O 1s intensity in Fig. 2(a) about a mean value follows very closely the behavior of δ, a point to which we return below. Proceeding now via the Fresnel equations to calculate the photoemission intensity as a function of photon energy, it can be shown that, for p-polarized radiation incident on a planar surface from vacuum with $n=1$, and for a conducting or nonconducting, but nonmagnetic, reflective medium, the ratio of the complex electric field magnitude just below the surface $[E(z=0+)]$ to the incident complex field magnitude just above the surface in vacuum $[E_{vac}^{inc}(z=0-)]$ is given by

$$t\equiv\frac{E(0+)}{E_{vac}^{inc}(0-)}=\frac{2\sin\theta_{h\nu}}{\sin\theta'_{h\nu}+n_r\sin\theta_{h\nu}}, \quad (12)$$

where z is the coordinate perpendicular to the surface and $\theta'_{h\nu}$ is the complex angle of propagation below the surface, again measured relative to the surface. $\theta'_{h\nu}$ is further related

to $\theta_{h\nu}$ via Snell's Law: $\cos\theta_{h\nu}=n_r\cos\theta'_{h\nu}$, with $\theta_{h\nu}$ real. The complex character of n_r also implies that E attenuates with z only according to $\exp[-\text{Im}(k'z\sin\theta'_{h\nu})]$, where k' is the complex propagation wave vector inside the medium and equal to $2\pi n_r/\lambda_x$, and λ_x is the wavelength of the radiation. Normalizing the electric field inside the medium to the incident field just above the surface then gives for the electric field strength at depth z relevant for photoemission

$$|E(z)|^2=|t|^2\exp(-\text{Im}\{4\pi n_r z\sin\theta'_{h\nu}/\lambda_x\}). \quad (13)$$

The photoemission intensity $I(h\nu)$ can now be obtained by introducing the energy-dependent differential photoelectron cross section $d\sigma/d\Omega$ appropriate to the experimental geometry (which may in general also include the effects of photoelectron diffraction), the energy-dependent inelastic attenuation length for electrons Λ_e, and integrating over z as

$$I(h\nu)\propto\frac{d\sigma}{d\Omega}\int_0^\infty|E(z)|^2\exp\left(-\frac{z}{\Lambda_e\sin\theta}\right)dz, \quad (14)$$

where we have not included factors of atomic density and solid angle acceptance of the analyzer that will be constant over an energy scan. Substituting Eq. (13) into Eq. (14) and integrating then yields finally

$$I(h\nu)\propto\frac{d\sigma}{d\Omega}(h\nu)$$

$$\times\frac{|t(h\nu)|^2}{\dfrac{\text{Im}\{4\pi n_r(h\nu)\sin\theta_{h\nu}'(h\nu)\}}{\lambda_x(h\nu)}+\dfrac{1}{\Lambda_e(h\nu)\sin\theta}}, \quad (15)$$

which is a completely general formula for photoemission intensity from a conducting or nonconduction, nonmagnetic, semi-infinite substrate, with all dependences on energy explicitly indicated. Making use of Eq. (15) and the experimental values for δ and β in Fig. 2(b), we arrive at the dashed curve in Fig. 2(a), which is in excellent agreement with experiment, including all aspects of the fine structure. A similar degree of agreement is also found for other incidence angles $\theta_{h\nu}$.

This x-ray optical approach furthermore exhibits only small differences in fine structure with respect to the microscopic description based upon Eq. (11). These differences are due to differences in δ and β between theory and measurement [cf. Fig. 2(b)] and perhaps also to the fact that only the Mn polarizability has been considered in the microscopic theory, thus neglecting the small contributions from nonresonant O scattering over this energy range.[30b,31] In addition, we find that, if the infinite-order microscopic Eq. (11) is used together with the experimental x-ray optical constants to derive the polarizability, the calculated curve is essentially indistinguishable from that of Eq. (15), thus verifying the accuracy of the microscopic approach and its exact reduction to the x-ray optical model, provided that multiple scattering effects are included and certain conditions mentioned above are met.

In Fig. 2(c), we finally show normalized curves of the multiatom effect on the O $1s$ intensity as a function of an x-ray incidence angle, as calculated using the x-ray optical approach of Eq. (15). These curves make it clear that the effects are strongly sensitive to an x-ray incidence angle, being much smaller for angles greater than about 30°, although very similar in shape for all angles. The calculated normalized $+/-$ excursion of the effect as a function of an incidence angle is further shown in the inset of Fig. 2(c), where it is compared to experimental results at four incidence angles. There is excellent agreement between experiment and theory, and theory furthermore predicts an asymptotic value of about 4.5% for the excursion at normal incidence. These results thus further confirm the accuracy of the x-ray optical analysis as compared to experiment, and also imply that such effects should be observable on crossing strong core-level resonances for *all* angles of x-ray incidence, although with greater difficulty of observation as $\theta_{h\nu}$ goes above about 20–30°.

We also note that recent measurements have found similar MARPE effects in O $1s$ emission from CuO with Cu $2p_{3/2}$ resonance, and these show a overall excursion of $\sim$20% that is similar to the magnitudes observed here for MnO.[13] Here, the effects have been termed ''anti-resonances'' to distinguish them from the all-positive effects reported in previous uncorrected data [cf. Fig. 1(c)], but the present paper makes it clear that they are manifestations of the same interatomic resonant phenomenon. Although it was not possible in this paper to see similar effects in O $1s$ emission from NiO,[13] we believe that this could be due to the relatively high x-ray incidence angle of 35° used in this paper, combined with the $\sim\pm2\%$ statistical error in the data as compared to the few percent effect that might be expected at this incidence angle [cf. inset of Fig. 2(c)].

It is now useful to compare these theoretical results with those from prior work by Henke on calculating photoelectron intensities via x-ray optics.[30a] We first note that he was interested in scanning the incidence angle $\theta_{h\nu}$ only, in which case δ, β, λ_x, and Λ_e all remain constant, and he was thus able to make certain approximations that we cannot, due to the strong variation of both δ and β over a scan in photon energy. Nonetheless, if $|\delta|,\beta\ll 1$ over the energy scan, which Fig. 2(b) makes clear is an excellent assumption, our Eq. (15) can be simplified to

$$I(h\nu)\approx\frac{d\sigma}{d\Omega}(h\nu)$$

$$\times\frac{|t(h\nu)|^2}{\dfrac{4\pi\beta(h\nu)\sin\theta_{h\nu}(h\nu)}{\lambda_x(h\nu)}+\dfrac{1}{\Lambda_e(h\nu)\sin\theta}}, \quad (16)$$

which permits more direct comparison with this prior work. In particular, our use of $|t|^2$ to represent the strength of the electric field squared below the surface is inherently more accurate and versatile in application than the factor $[1-R]$ $\times[\sin\theta_{h\nu}/\sin\theta_{h\nu}']$ used by Henke in his prior analysis. An additional difference in the two approaches is that all quantities in the last expression are treated as real by Henke, whereas we have shown that a more accurate expression re-

lated to this earlier formalism is a factor $[I-R][\sin\theta_{h\nu}/(\text{Re}\{n_r\sin\theta'_{h\nu}\})]$, with n_r and $\theta_{h\nu}'$ here treated as complex. In addition, the inverse x-ray attenuation length perpendicular to the surface in this prior work and appearing here as the first term in the denominator of Eq. (16) was further simplified by Henke, and finally is different from ours by a factor of $1/[\sin\theta_{h\nu}']^2$. In describing scanned-energy resonant data however, we find it essential to use the form in Eq. (15), or with some approximation, that in Eq. (16).

To gain further insight into the relationship of photoemission intensity of δ and β, we can further approximate Eq. (15) to the conditions of the measurements shown here, for which δ and β are both much less than unity [cf. Fig. 2(b)] and the reflectivity R is also small (with a maximum value for all cases considered here of 0.18 at $\theta_{h\nu}=5°$), and this finally yields, after suppressing the obvious dependences on photon energy

$$I(h\nu)\approx\frac{d\sigma}{d\Omega}\frac{1+\delta}{\dfrac{4\pi\beta\sin\theta_{h\nu}}{\lambda_x}+\dfrac{1}{\Lambda_e\sin\theta}}. \qquad (17)$$

From this expression, it is clear that the variation of intensity with photon energy as normalized to the values on either side of a resonance should qualitatively follow δ, just as observed. The magnitude of this variation is also enhanced by the change in β, whose increase over the resonance generally acts to decrease intensity over the same region. The negative excursion of δ just before the resonance, together with the increase in β, thus produces the strong dips in intensity seen at about 639.5 eV in Figs. 2(a) and 2(d).

Although the numerical results from the microscopic model embodied in Eqs. (1)–(11) can be reduced to a continuum x-ray optical picture, provided we include higher-order effects representing multiple light scattering, it should nonetheless permit future calculations of such interatomic resonant photoemission effects from first principles, including in particular, an allowance for nearest-neighbor many-body interactions that are only effectively included in the optical approach. Of course, any microscopic model is in a sense simply calculating the x-ray optical response of the system, but for nearest-neighbor effects, in free molecules, and for small clusters of atoms on the nanometer scale, it is not clear that an x-ray optical approach is particularly useful, or even appropriate. Beyond this, the excellent numerical agreement between the microscopic and macroscopic continuum dielectric descriptions presented above is expected to break down when the wavelength of the radiation is of the order of, or smaller than, the relevant interatomic distances. Thus, if the resonating atoms do not form a compact enough lattice (as Mn does in MnO), the continuum dielectric treatment is not appropriate. Some possible examples of this are atoms situated inside the cages of fullerites or zeolites, and/or systems subjected to resonant excitation by shorter-wavelength radiation. The continuum dielectric model also is not appropriate for calculating such effects in nanometer-scale objects or systems with nanometer-scale heterogeneity or clustering in which the detailed atomic positions are to be allowed for, even if this model can be extended via methods

such as the Mie theory so as to apply to special cases such as small metal clusters of regular shape.[34] Neither is the continuum model appropriate for free molecules, in which core-core interatomic resonance effects appear to have recently been observed in angular distributions.[12]

We also comment briefly on an intermediate theoretical approach that would involve assigning each atom a complex scattering factor based on some combination of measured and/or calculated optical constants, somehow partitioned among the different constituents so as to allow for element-specific resonance effects, with standard formulas for this appearing elsewhere.[30b] This method could in principle be applied to any arbitrary cluster of atoms, and with sufficient long-range order, would lead to Bragg scattering effects at shorter wavelengths. However, this approach could not incorporate any unique nearest-neighbor effects, nor in its standard formulation would it explicity allow for the multiple scattering effects on resonance that we find to be important.

Regardless of the theoretical model that is most appropriate to use, such interatomic resonance effects (even though generally smaller and of different form than discussed previously) still represent an experimental probe that should be able, for various situations, to provide information on the near-neighbor identities and bonding of atoms B that surround a given emitter A, as suggested in prior work.[1–4]

Finally, we note that both of the theoretical models discussed above can be extended to describe fluorescent x-ray emission. For the x-ray optical model, and for the case of a fluorescent energy that is far from any resonance and at a fluorescence exit angle θ^F that is large enough to minimize refraction and reflection at the surface, this would involve simply replacing $\Lambda_e\sin\theta$ with $\Lambda_x^F\sin\theta^F$ in Eqs. (15)–(17), with Λ_x^F equal to the fluorescent x-ray attenuation length along path length or $\lambda_x^F/[4\pi\beta^F]$ in obvious notation. With this replacement, Eqs. (15)–(17) thus represent different levels of approximation for handling what essentially reduces to the well-known self-absorption effects in x-ray fluorescence that have been discussed previously in connection with MARPE.[4,14] In fact, viewed in this light, MARPE in x-ray emission can be seen as having self-absorption as a key ingredient, but due to near-neighbor effects not the only ingredient. The microscopic model could also be similarly extended to predict fluorescence intensities, but we will not present these details here.

V. CONCLUSIONS

In summary, we have pointed out that a proper allowance for detector nonlinearity is essential for accurately measuring multiatom resonant photoemission effects, with the magnitude and form of the corrected results being significantly different from previous reports.[1–4,6,7a] A microscopic theoretical model proposed previously for describing these results[5] is found to well describe the observed effects, and confirms, via agreement with experiment, that they can be considered as interatomic resonance phenomenon. For the specific case of O $1s$ emission from MnO in the vicinity of the Mn$2p$ resonances treated here, this microscopic model, with the inclusion of higher-order interactions not considered previ-

ously, is also found to be reducible to a classical x-ray optical treatment using experimental optical constants. The x-ray optical model is furthermore found to well describe the observed intensity profiles as a function of both photon energy and x-ray incidence angle. It is thus of interest in future studies to explore the degree to which such effects (particularly with the expected enhancement of nearest-neighbor interactions, for more spatially dispersed resonating atoms so as to go beyond the simple x-ray optical picture, in nanometer-scale objects, and/or in free molecules) can provide an element-specific probe of near-neighbor properties and many-electron interactions. The experimental and theoretical approaches outlined here should provide a sound framework for such work, both for photoelectron and fluorescent x-ray emission. The microscopic theoretical model outlined here should also be capable of describing such core-core interatomic resonance effects in the intensities and angular distributions in photoemission from free molecules,[12] as well as with straightforward generalization the valence-core interatomic resonance effects mentioned previously.[8–10]

Finally, we point out that the demonstrated importance of multiple scattering of soft x-ray radiation in the vicinity of strong core-level resonances should be of relevance in the analysis of resonant elastic and inelastic x-ray scattering, and other topics of high current interest.[35]

[1] A. Kay, E. Arenholz, B. S. Mun, F. J. Garcia de Abajo, C. S. Fadley, R. Denecke, Z. Hussain, and M. A. Van Hove, Science **281**, 679 (1998).

[2] A. W. Kay, E. Arenholz, B. S. Mun, F. J. Garcia de Abajo, C. S. Fadley, R. Denecke, Z. Hussain, and M. A. Van Hove, J. Electron Spectrosc. Relat. Phenom. **103**, 647 (1999).

[3] (a) C. S. Fadley, E. Arenholz, A. W. Kay, J. Garcia de Abajo, B. S. Mun, S.-H. Yang, Z. Hussain, and M. A. Van Hove, in *X-ray and Inner-Shell Processes*, edited by R. W. Dunford, D. S. Genmell, E. P. Kanter, B. Krässig, S. H. Southwartor, and L. Young, AIP Conf. Proc. No. 506 (AIP, Melville, NY, 2000), pp. 251–272; (b) E. Arenholz and A. W. Kay (unpublished).

[4] E. Arenholz, A. W. Kay, C. S. Fadley, M. M. Grush, T. A. Callcott, D. L. Ederer, C. Heske, and Z. Hussain, Phys. Rev. B **61**, 7183 (2000).

[5] F. J. Garica de Abajo, C. S. Fadley, and M. A. Van Hove, Phys. Rev. Lett. **82**, 4126 (1999).

[6] A. Kikas, E. Nommiste, R. Ruus, A. Saar, and I. Martinson, Solid State Commun. **115**, 275 (2000).

[7] (a) M. G. Garnier, N. Witkowski, R. Denecke, D. Nordlund, A. Nilsson, M. Nagasono, N. Mårtensson, and A. Föhlisch, Maxlab Annual Report for 1999 and (private communication) correcting this data; (b) D. Nordlund, M. G. Garnier, N. Witowsky, R. Denecke, A. Nilsson, M. Nagasono, N. Mårtensson, and A. Föhlisch (unpublished).

[8] K. L. I. Kobayashi, N. Watanabe, H. Nakashima, M. Kubota, H. Daimon, and Y. Murata, Phys. Rev. Lett. **52**, 160 (1984).

[9] P. Pervan, M. Milun, and D. P. Woodruff, Phys. Rev. Lett. **81**, 4995 (1999).

[10] Y. F. Hu, G. M. Bancroft, and K. H. Tan, Inorg. Chem. **39**, 1255 (2000).

[11] S.-H. Yang, B. S. Mun, A. W. Kay, S.-K. Kim, J. B. Kortright, J. H. Underwood, Z. Hussain, C. S. Fadley, Surf. Sci. **461**, 557 (2000).

[12] H. Wang, O. Hemmers, P. Focke, M. M. Sant'Anna, D. Lukic, C.

Heske, R. C. C. Perera, I. Sellin, and D. Lindle (unpublished).

[13] M. Finazzi, G. Ghiringhelli, O. Tjernberg, L. Duo, A. Tagliaferri, P. Ohressser, and N. B. Brookes (unpublished).

[14] A. Moewes, E. Z. Kurmaev, D. L. Ederer, and T. A. Callcott (unpublished).

[15] (a) N. Mårtensson, P. Baltzer, P. A. Bruhwiler, J. -O. Forsell, A. Nilsson, A. Stenborg, and B. Wannberg, J. Electron Spectrosc. Relat. Phenom. **70**, 117 (1994); (b) C. S. Fadley, Prog. Surf. Sci. **54**, 341 (1997).

[16] M. P. Seah, I. S. Gilmore, and S. J. Spencer, J. Electron Spectrosc. Relat. Phenom. **104**, 73 (1999), and earlier references therein.

[17] A. W. Kay, Ph.D. dissertation, University of California-Davis, 2000, Chap. 4 and 5.

[18] A. Gromko, C. Yi, A. Fedorov, and D. Dessau (private communication).

[19] T. Valla and P. D. Johnson (private communication).

[20] J. J. Yeh and I. Lindau, At. Data Nucl. Data Tables **32**, 1 (1985).

[21] C. S. Fadley, Prog. Surf. Sci. **54**, 341 (1997), and references therein.

[22] F. J. Garía de Abajo, M. A. Van Hove, and C. S. Fadley, Phys. Rev. B (to be published).

[23] A. Messiah, *Quantum Mechanics* (North-Holland, New York, 1969), Vol. II, p. 849.

[24] A. Tanaka and T. Jo, J. Phys. Soc. Jpn. **63**, 2788 (1994).

[25] N. F. Mott and I. N. Sneddon, *Wave Mechanics and its Applications* (London, Oxford University Press, 1948), pp. 338–339.

[26] J. P. Desclaux, in *Relativistic Effects in Atoms, Molecules, and Solids*, edited by G. L. Malli (Plenum Press, New York, 1981), pp. 115–143.

[27] The Gaunt normalization is chosen such that $\langle Y_{1\mu}|Y_{1\lambda}Y_{00}\rangle =$ the integral over solid angle Ω of $Y_{1\mu}^{*}(\Omega)Y_{1\lambda}(\Omega)Y_{00}(\Omega) = \delta(\mu,\lambda)/\sqrt{4\pi}$.

[28] Y. Nishino and G. Materlik, Phys. Rev. B **60**, 15 074 (1999).

[29] C. Cohen-Tannoudji, J. Dupont-Roc, and G. Grynberg, *Photon &*

Atoms. Introduction to Quantum Electrodynamics (Wiley, New York, 1989).

[30] (a) B. L. Henke, Phys. Rev. A **6**, 94 (1972); (b) B. L. Henke, E. M. Gullikson, J. C. Davis, At. Data Nucl. Data Tables **55**, 34 (1993).

[31] C. T. Chantler, J. Phys. Chem. Ref. Data **24**, 71 (1995).

[32] The sign convention for the imaginary part of the index of refraction used here is different from that used elsewhere of $n_r = 1 - \alpha - i\beta$ (Refs. 25, 27), but we choose it to be consistent with the use of retarded Green functions for G_0.

[33] G. van der Laan and B. T. Thole, J. Electron Spectrosc. Relat. Phenom. **46**, 123 (1988).

[34] S. V. Fomichev and D. F. Zaretsky, J. Phys. B **32**, 5083 (1999), and references therein.

[35] P. M. Platzman and E. D. Isaacs, Phys. Rev. B **57**, 11 107 (1998); P. Kuiper, J. H. Guo, C. Sathe, J. Nordgren, J. J. M. Pothuizen, F. M. F. deGroot, and G. A. Sawatzky, Phys. Rev. Lett. **80**, 5204 (1998).